HAL
open science

Study of ion-implanted nitrogen related defects in diamond Schottky barrier diode by transient photocapacitance and photoluminescence spectroscopy

Junjie Guo, Aboulaye Traore, Masahiko Ogura, Muhammad Hafiz Bin Abu Bakar, Satoshi Yamasaki, Etienne Gheeraert, Toshiharu Makino, Takeaki Sakurai

To cite this version:

Junjie Guo, Aboulaye Traore, Masahiko Ogura, Muhammad Hafiz Bin Abu Bakar, Satoshi Yamasaki, et al.. Study of ion-implanted nitrogen related defects in diamond Schottky barrier diode by transient photocapacitance and photoluminescence spectroscopy. Japanese Journal of Applied Physics, 2021, 60 (SB), pp.SBBD07. 10.35848/1347-4065/abdf75 . hal-03167465

HAL Id: hal-03167465

https://hal.science/hal-03167465

Submitted on 18 Mar 2021

HAL is a multi-disciplinary open access archive for the deposit and dissemination of scientific research documents, whether they are published or not. The documents may come from teaching and research institutions in France or abroad, or from public or private research centers.

L'archive ouverte pluridisciplinaire **HAL**, est destinée au dépôt et à la diffusion de documents scientifiques de niveau recherche, publiés ou non, émanant des établissements d'enseignement et de recherche français ou étrangers, des laboratoires publics ou privés.

Study of ion-implanted nitrogen related defects in diamond Schottky barrier diode by transient photocapacitance spectroscopy

Junjie Guo[1,2], Aboulaye Traore[1], Masahiko Ogura[2], Muhammad Hafiz Bin Abu Bakar[1,2], Satoshi Yamasaki[1,2,4], Etienne Gheeraert[1,3], Toshiharu Makino[1,2] and Takeaki Sakurai[1]*

[1]*Pure and Applied Sciences, University of Tsukuba, 1 Chome-1-1 Tennodai, Tsukuba, Ibaraki 305-8577, Japan*

[2]*Advanced Power Electronics Research Center, National Institute of Advanced Industrial Science and Technology (AIST), 1-chōme-1-1, Umezono, Tsukuba, Ibaraki 305-8560, Japan*

[3] *Université Grenoble Alpes, 621 avenue Centrale 38400 Saint-Martin-d'Hères, France*

[1] *Kanazawa University, Kakumamachi, Kanazawa, Ishikawa, 920-1192, Japan*

E-mail: s1930098@s.tsukuba.ac.jp, sakurai@bk.tsukuba.ac.jp

The study of nitrogen-vacancy (NV) centers in diamond films are growing attractive in the application of quantum devices. Here, electrical control of NV charge state and defects induced by nitrogen ions implantation in diamond films were investigated by transient photocapacitance (TPC) spectroscopy and photoluminescence (PL) spectroscopy. The experiments show that thresholds of 1.2 eV appeared in TPC spectra are probably due to the presence of excited defect energy levels related to vacancy or NV center. Alternatively, the 2.2 eV defect observed in the TPC spectrum is probably attributed to the NV centers. The variation of PL spectra with different applied voltages suggests that bias voltages control the charge state of the NV centers since their effect on the Fermi level shifting in the depletion region.

1. Introduction

Nitrogen-vacancy (NV) centers in diamond films are intensively investigated for the accomplishment of quantum devices because of the optical addressing and microwave control of their spin state even at room temperature[1-4]. Nowadays, the widely used method to produce NV center is the nitrogen ion implantation followed by annealing at high temperature, controlling their distribution by changing the energy and dose of nitrogen ions[5-7]. For the applications, the charge state control of the NV centers is crucial[8-10], because the realization of individually addressable spins of the NV centers is only possible in a negative charge state[1, 3]. And a fast switching between different charge states is also very important[11]. One problem is that surface terminations and defects affect the near-surface NV centers[12, 13].

In this research, electrical control of NV center charge state and defects induced by nitrogen ions implantation in the diamond are investigated by transient photocapacitance (TPC) spectroscopy and photoluminescence (PL) spectroscopy. Because of the pretty wide bandgap of the diamond up to 5.5 eV[14], it is difficult to detect the defects without photoexcitation[15, 16]. TPC spectroscopy and photocurrent spectroscopy are good choices as the most sensitive methods for diamond semiconductor defect testing[16-18]. Although both measurements are sensitive to deep levels in diamond, one thing must be noted that the recombination may affect the result, since there are two signs of free carriers in photocurrent spectroscopy[19, 20]. However, it is different in TPC spectroscopy. Electron and hole transitions give opposite sign signals, so it may readily observe the optical and thermal excitation processes[19, 20]. And the other important point is that photocapacitance detects only the net charge variation in the depletion region[21]. Besides, since the NV center is optically active, the identification of the charge state of NV centers can be realized by PL spectoscopy[8, 22]. We have previously used transient photocapacitance spectroscopy to detect defects in diamond Schottky diodes[23]. Here, by applying different reverse bias, the TPC spectrums and PL of ion-implanted diamond films were measured. From the achieved spectrums, electrical control of the NV center charge state was discussed. The optical

transition process of defects was investigated by Steady-state photocapacitance measurement.

2. Experimental methods

A high-pressure/high-temperature IIb diamond substrate (001) (with an off-angle of 3.5°) was used to fabricate the vertical Schottky barrier diodes. A 1 μm thick slightly boron-doped ($3*10^{16}\ \ cm^{-3}$) the homoepitaxial diamond layer was grown on the substrate using microwave plasma chemical vapor deposition technique (MPCVD)[24].

After the deposition, half of the diamond epitaxial layer was nitrogen ion-implanted with an energy of 80 keV equivalent to a mean depth of 100 nm according to an SRIM simulation and with a dose of $10^{12}\ \ ions/cm^2$ at 600 ℃. The SRIM simulation result was shown in figure 1. The sample was annealed for 1 h at 1000 ℃ to create Nitrogen-Vacancy centers. From S. Pezzagna's report[25], they experimentally showed that the creation efficiency of NV centers largely depends on the implanted ion energy. In the 80 keV case, the production efficiency of NV centers is around 10%. After that, we deposited sandwich structure contacts using a photolithography technique, several Schottky electrodes with 10 nm thick Mo (300 μm in diameter) evenly on the whole surface, and Ohmic electrode with Ti (30 nm)/Pt (30 nm)/Au (100 nm) on the whole backside. The Ti/Pt/Au electrode was annealed for 30 min at 420 ℃ to give rise to Ohmic properties by forming titanium carbide[26]. As Schottky electrodes, Mo electrodes were fabricated after UV ozone treatment, which can form oxygen-termination diamond surface[27].

In other words, the Schottky diodes fabricated on CVD boron-doped diamond layer were divided into two parts, with and without nitrogen implantation. Figure 2 shows (a) the schematic diagram of the sample structure, and (b) the top view of the sample. In figure 1(b), the part covered by shadows is the area without ion implantation, and the small bright yellow circle is the gold (100nm) deposited on the electrode for the wire bonding.

Photocapacitance spectra were measured with the illumination of a halogen lamp

(wavelength, 400-1200nm), based on a monochromator setup. The Schottky electrode was covered by the light spot. The transmittance of the 10 nm Mo electrode is above 50%[28]. Before the measurements, the Schottky diode was relaxed under dark conditions for a sufficiently long time at room temperature. An electronic shutter controls the on and off of the illumination on the sample. The TPC signals were executed by a Boonton 72B capacitance meter with a frequency of 1 MHz with a quiescent bias of a reverse bias voltage and a filling pulse bias of 0V. The pulse width and duration were 500 ms and 10 s, respectively.

3. Results and discussion

3.1 The transient photocapaitance spectroscopy

Figure 3 shows the current-voltage characteristics of both areas in the diamond Schottky barrier diodes. The red and black curves are signals of Schottky diodes fabricated in the areas with and without ion implantation, respectively. The large difference between the forward current and leakage current indicates that the Schottky barrier diodes have good rectification properties. Details of diode parameters are shown in Table I. A lower forward current in the implantation area is because of higher defect density which affected effective carrier concentration and diode series resistance[29]. A large value of the ideality factor n (for an ideal diode n=1) in without implantation area can be attributed to the presence of the interface, series resistance, etc[30]. In the implantation area, the implantation of nitrogen into the p-type diamond film may form an intrinsic region, the ideality factor exceeds the theoretical value of 2 when the recombination is extended to a wide region[31].

Figure 4 shows the TPC signals normalized by the photon flux (S_{TPC}) as a function of the photon energy. The red and black curves are TPC signals of Schottky diodes fabricated in the areas with and without ion implantation, respectively. There are two thresholds in the red curve, which is probably because of the existence of excited defect energy levels. The spectra were fitted with a Lucovsky function for photoionization cross section[32, 33]:

$$\sigma_{hv} \propto \frac{(hv-E_t)^{\frac{3}{2}}}{hv^3} \quad (1)$$

where hv photon energy, E_i photoionization energy of the defect.

The obvious increase from around 1.2 eV of photocapacitance in spectra should be due to the hole emission from traps in the depletion region of the Schottky diodes. The threshold of 1.2 eV appears in both signals, where the intensity of the signal in the implantation area is higher. However, it was found in the report from Zeisel et al that even in synthetic type IIb diamond, a defect at corresponding energy could be detected [15]. So that means the 1.2 eV defect signal can be enhanced by nitrogen implantation and the possible chemical candidate may be assigned as vacancy or NV center. The 2.2 eV defect only exists in the implantation area, which probably is attributed to the NV center. Because the observed absorption and the zero phonon line (ZPL) energy of the NV center were obtained in Weber et al.'s reports[34], which is 2.27 eV and 2.02 eV, and also in good agreement with some previous experiment[35] as well as with calculations[36].

It was known that the charge state of NV centers varies with different biases because of the variation of the Fermi level in the depletion region[8, 37]. To try electrical control of the NV center, TPC spectroscopy was measured under different quiescent biases (reverse bias), as shown in figure 5. From G. M. Matain's reports[38], the transient photocapacitance is increasing with higher reverse bias. The experimental result below 2.2 eV is a good agreement to it. However, after 2.2 eV, the spectrum shape changed, the capacitance is not increasing with higher bias. It is assumed that the change is from the variation of the charge state of NV centers. When applying reverse bias, the Fermi level may cross the $NV^{+/0}$ level, some NV^+ change to NV^0[11]. Another assumption is the distribution of the NV center at 100nm. The ratio of NV distribution and depletion layer may affect the result.

3.2 The photoluminescence spectroscopy

The PL spectra have been measured under different bias conditions to identify the electrical control of the charge state of NV centers as shown in figure 6. At zero bias, since the NV centers are mainly the NV^+ and NV^0 in the boron-doped diamond film, there is only an NV^0 signal with the characteristic ZPL at 575 nm, and its phonon

sideband (black spectrum in Figure 6). By applying the reverse bias of -10 V, the intensity of NV^0 signal slightly decreases without noticeable difference of spectrum shape (pink spectrum in Figure 6). When increasing the reverse bias to -20 V and -30 V, the PL spectra show clear NV^- signals with the characteristic ZPL at 637 nm and its phonon sideband and the intensity of the NV^0 signal drastically changed (blue and green spectrum in Figure 6).

The variation of PL spectra with different applied voltages suggests that applying different bias voltages can control the charge state of NV centers due to their effect on the Fermi level in the depletion region of Schottky contact. The band diagram was shown in figure 7, for 0 bias, since the Fermi level is around the $NV^{+/0}$ transition level, the NV centers are mainly NV^0 and NV^+. When applying reverse biases on Schottky contact, the Fermi level starts to cross the $NV^{+/0}$ and then the $NV^{0/-}$, so the NV centers become from NV^+ to NV^0 and then to NV^-. Between 0 V and -10 V, there is only NV^0 intensity change but not spectrum shape changes, which is because NV^- is not saturated at all. For this reason, it was assumed that the change of NV^+ and NV^0 concentration may influence the TPC result with different reverse biases.

3.3 The steady-state photocapacitance

To investigate the optical transition property of 2.2 eV defect observed in TPC spectroscopy, steady-state photocapacitance as a function to time with a wavelength of 564nm was measured under 0 bias and reverse bias. The results were displayed in figure 8. Under 0 bias, as shown in the black curve in figure 8, the capacitance gradually increases under illumination, which is caused by the capture of electrons from the valence band into 2.2 eV level (release of holes from 2.2 eV level to the valence band). This process lasted over twenty minutes and still did not reach a stable state. It can be seen that because the energy level in diamond is too deep, the time it takes for electrons to fill the trap is very long.

The amplitude of the photocapacitance transient can be given as follows[16, 39].

$$\Delta C = \frac{C_0 N_t}{2N_A} \tag{2}$$

Where C_0 the junction capacitance of the Schottky diode under dark condition, N_t the

trap density, and N_A the acceptor density. However, one thing to note is that in our sample, part of the area on the Schottky electrodes was covered by gold for wire bonding, the light cannot completely penetrate the entire Schottky electrode. But the capacitance measured the change of net charges in the entire depletion layer under the electrode. So here, the exact value of the transient photocapacitance is not convincing enough, it can be only roughly estimated the order of magnitude of defect density and the photoionization cross-section. The obtained defect density (Nt) based on Eq. (2) is on the order of 10^{15} cm^{-3}, which is a good agreement with 10% of the SRIM simulation result of nitrogen ion implantation[25]. Then the photoionization cross-section is on the order of 10^{-15} cm^2.

After the light stops, in addition to the non-equilibrium carrier recombination through the recombination center, the carrier in the trap is gradually released and recombination to reach the equilibrium state. Therefore, when the light stops, the photocapacitance decay time will increase significantly. Especially for the trap with the deep energy level in wide bandgap semiconductors, the thermal excitation rate of the trapped carrier is minimal, and then the photocapacitance decay time will depend on the slow electron release process, sometimes very long.

The red curve in figure 8 shows the steady-state photocapacitance results with applied reverse bias. Under the light, the time for electrons to fill the trap is significantly reduced due to the applied reverse voltage. Compared with more than 20 min under 0 bias, it only takes about 12 s to reach the stable state photocapacitance after applying reverse bias. After stopping the light, the time for electrons to release from the trap is also greatly reduced. It is very obvious that when applying bias, a higher electrical field enhances the process of filling and releasing, the decay time decreases[40].

4. Conclusions

Electrical control of NV center charge state and defects induced by nitrogen ions implantation in diamond films has been investigated by transient photocapacitance (TPC) spectroscopy and photoluminescence (PL) spectroscopy. Defect levels at 1.2 eV

and 2.2 eV were detected in the implanted diamond layer. It is assumed that 1.2 eV defect is related to vacancy or NV center and 2.2 eV is contributed to the NV center. The change of charge state of the NV centers or the ratio of the distribution of NV center and depletion layer affect TPC results with different biases. By applying different biases on the Schottky contact and simultaneous illumination (532 nm laser light), NV centers can be actively transported between the negative state and natural state. It is due to the Fermi level shifts around defect levels, which varied the charge state of the carrier and its electrical and optical properties. On the other hand, it is found that the 2.2 eV deep trap in diamond slow down the process of photocapacitance rise and fall, but a higher electrical field can enhance the process of filling and releasing, and decrease the decay time.

Acknowledgments

The technicians in AIST and colleagues at the University of Tsukuba and the University of Grenoble supported a lot in this work. The authors gratefully acknowledge their support.

References

1) M.W. Doherty, N.B. Manson, P. Delaney, F. Jelezko, J. Wrachtrup and L.C.L. Hollenberg, Physics Reports. **528**, 1, (2013).

2) F.J. Heremans, C.G. Yale and D.D. Awschalom, Proceedings of the IEEE. **104**, 2009, (2016).

3) D. Hopper, H. Shulevitz and L. Bassett, Micromachines. **9**, (2018).

4) S. Choi, M. Jain and S.G. Louie, Physical Review B. **86**, (2012).

5) A. Haque and S. Sumaiya, Journal of Manufacturing and Materials Processing. **1**, (2017).

6) J. Meijer, B. Burchard, M. Domhan, C. Wittmann, T. Gaebel, I. Popa, F. Jelezko and J. Wrachtrup, Applied Physics Letters. **87**, (2005).

7) D.M. Toyli, C.D. Weis, G.D. Fuchs, T. Schenkel and D.D. Awschalom, Nano Letters. **10**, 3168, (2010).

8) C. Schreyvogel, V. Polyakov, R. Wunderlich, J. Meijer and C.E. Nebel, Sci Rep. **5**, 12160, (2015).

9) B. Grotz, M.V. Hauf, M. Dankerl, B. Naydenov, S. Pezzagna, J. Meijer, F. Jelezko, J. Wrachtrup, M. Stutzmann, F. Reinhard and J.A. Garrido, Nat Commun. **3**, 729, (2012).

10) C. Schreyvogel, M. Wolfer, H. Kato, M. Schreck and C.E. Nebel, Sci Rep. **4**, 3634, (2014).

11) C. Schreyvogel, V. Polyakov, S. Burk, H. Fedder, A. Denisenko, F. Favaro de Oliveira, R. Wunderlich, J. Meijer, V. Zuerbig, J. Wrachtrup and C.E. Nebel, Beilstein J Nanotechnol. **7**, 1727, (2016).

12) L. Rondin, G. Dantelle, A. Slablab, F. Grosshans, F. Treussart, P. Bergonzo, S. Perruchas, T. Gacoin, M. Chaigneau, H.C. Chang, V. Jacques and J.F. Roch, Physical Review B. **82**, (2010).

13) K.M.C. Fu, C. Santori, P.E. Barclay and R.G. Beausoleil, Applied Physics Letters. **96**, (2010).

14) C.J.H. Wort and R.S. Balmer, Materials Today. **11**, 22, (2008).

15) R. Zeisel, C.E. Nebel and M. Stutzmann, Journal of Applied Physics. **84**, 6105, (1998).

16) O. Maida, T. Hori, T. Kodama and T. Ito, Materials Science in Semiconductor Processing. **70**, 203, (2017).

17) M. Nesládek, L.M. Stals, A. Stesmans, K. Iakoubovskij, G.J. Adriaenssens, J. Rosa and M. Vaněček, Applied Physics Letters. **72**, 3306, (1998).

18) K. Murayama, N. Kodaira, T. Makino, T. Kubo, M. Ogura, S. Ri, D. Takeuchi, S. Yamasaki and H. Okushi, Diamond and Related Materials. **15**, 577, (2006).

19) A.V. Gelatos, K.K. Mahavadi, J.D. Cohen and J.P. Harbison, Applied Physics Letters. **53**, 403, (1988).

20) J.T. Heath, J.D. Cohen, W.N. Shafarman, D.X. Liao and A.A. Rockett, Applied Physics Letters. **80**, 4540, (2002).

21) X. Hu: Doctor, Study of deep-level defects in Cu(In, Ga)Se2 thin film grown by three-stage process, University of Tsukuba, 2015.

22) A. Gruber, A. Drabenstedt, C. Tietz, L. Fleury, J. Wrachtrup and C. vonBorczyskowski, Science. **276**, 2012, (1997). [in English].
23) J. Guo, A. Traore, M.H.B.A. Bakar, T. Makino, S. Yamasaki, M. Ogura and T. Sakurai, Solid State Devices and Materials 2020. (2020).
24) M. Ogura, H. Kato, T. Makino, H. Okushi and S. Yamasaki, Journal of Crystal Growth. **317**, 60, (2011).
25) S. Pezzagna, B. Naydenov, F. Jelezko, J. Wrachtrup and J. Meijer, New Journal of Physics. **12**, (2010).
26) K.L. Moazed, R. Nguyen and J.R. Zeidler, IEEE Electron Device Letters. **9**, 350, (1988).
27) T. Ichibha, K. Hongo, I. Motochi, N.W. Makau, G.O. Amolo and R. Maezono, Diamond and Related Materials. **81**, 168, (2018).
28) S. Kang, R. Nandi, J.-K. Sim, J.-Y. Jo, U. Chatterjee and C.-R. Lee, RSC Adv. **7**, 48113, (2017).
29) A. Nawawi, K.J. Tseng, Rusli, G.A.J. Amaratunga, H. Umezawa and S. Shikata, Diamond and Related Materials. **35**, 1, (2013).
30) W. Shockley, *The Theory of p-n Junctions in Semiconductors and p-n Junction Transistors* (The Bell System Technical Journal, 1949).
31) M.A. Kroon and R.A.C.M.M. van Swaaij, Journal of Applied Physics. **90**, 994, (2001).
32) G. Lucovsky, Solid State Communications. **3**, 299, (1965).
33) L. Lugani, M.A. Py, J.F. Carlin and N. Grandjean, Applied Physics Letters. **109**, (2016).
34) J.R. Weber, W.F. Koehl, J.B. Varley, A. Janotti, B.B. Buckley, C.G. Van de Walle and D.D. Awschalom, Proc Natl Acad Sci U S A. **107**, 8513, (2010).
35) G.D.a.M.F. Hamer, Proceedings of the Royal Society of London. A. Mathematical and Physical Sciences. **348**, 285, (1997).
36) A. Gali, E. Janzen, P. Deak, G. Kresse and E. Kaxiras, Phys Rev Lett. **103**, 186404, (2009).
37) H. Kato, M. Wolfer, C. Schreyvogel, M. Kunzer, W. Müller-Sebert, H. Obloh, S. Yamasaki and C. Nebel, Applied Physics Letters. **102**, (2013).
38) G.M. Martin, A. Mitonneau, D. Pons, A. Mircea and D.W. Woodard, J Phys C Solid State. **13**, 3855, (1980). [in English].
39) C.E. Nebel, R. Zeisel and M. Stutzmann, physica status solidi (a). **174**, 117, (1999).
40) G.A.H. Wetzelaer, M. Kuik, H.T. Nicolai and P.W.M. Blom, Physical Review B. **83**, 165204 (2011).

Figure Captions

Fig. 1. SRIM simulation result of nitrogen ion implantation. Doze size is 10^{12} cm^{-2} and ion energy is 80 keV.

Fig. 2. (a) The schematic diagram of the sample structure, (b)the top view of the sample (the part covered by shadows is without ion implantation area, and the small bright yellow circle is the gold of 100nm deposited on the electrode for the wire bonding).

Fig. 3. Current-voltage characteristics of electrodes in both areas of the diamond Schottky barrier diodes at room temperature. The red and black curves are signals of Schottky diodes fabricated in the areas with and without ion implantation, respectively.

Fig. 4. The TPC spectroscopy of both areas in the diamond Schottky barrier diodes with illumination wavelengths from 400 nm to 1200 nm. The results were normalized by the photon flux (S_{TPC}). The red and black curves are TPC signals of Schottky diodes fabricated in the areas with and without ion implantation, respectively. The blue lines are the fitting results of the spectra by Eq. (1).

Fig. 5. The TPC spectroscopy under different quiescent biases (reverse bias). The filling pulse is 0 bias.

Fig. 6. The photoluminescence spectroscopy with different applied voltages using 532 nm green laser at room temperature.

Fig. 7. Band diagram of the depletion region in diamond Schottky barrier diode (a) at 0 bias,

(b) at -5 V and (c) -15 V. Fermi level (dot line) and the charge transition levels of NV centers (blue and green line) are shown.

Fig. 8. Steady-state photocapacitance as a function of time under 0 bias and reverse bias with the illumination of 564nm wavelength at room temperature.

Table I. Electrical properties of the Schottky barrier diodes.

	Dark saturation current I_S (A)	Series resistance R_S (Ω)	Ideality factor n
Without implantation area	$7.9*10^{-14}$	29.2	1.8
With implantation area	$2.4*10^{-13}$	1015.3	2.8

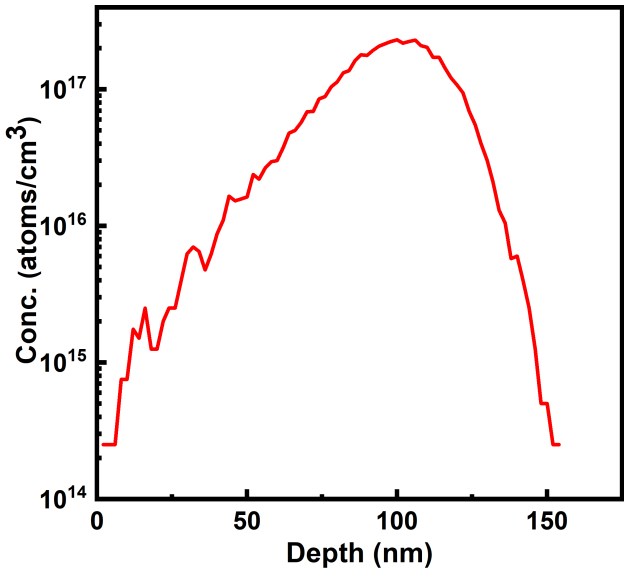

Figure 1

(a)

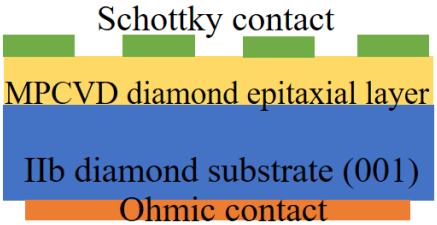
Schottky contact
MPCVD diamond epitaxial layer
IIb diamond substrate (001)
Ohmic contact

(b)

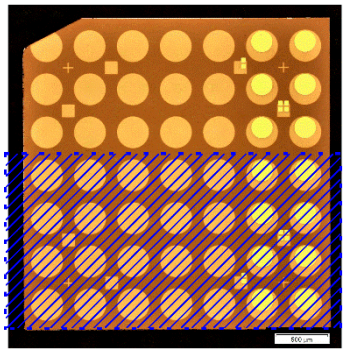

Figure 2

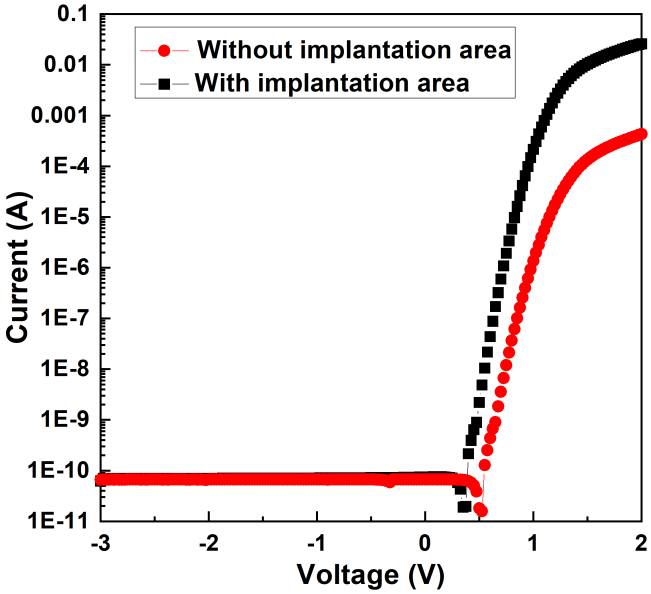
Without implantation area
With implantation area
Current (A)
Voltage (V)
0.1
0.01
0.001
1E-4
1E-5
1E-6
1E-7
1E-8
1E-9
1E-10
1E-11
-3
-2
-1
0
1
2

Figure 3

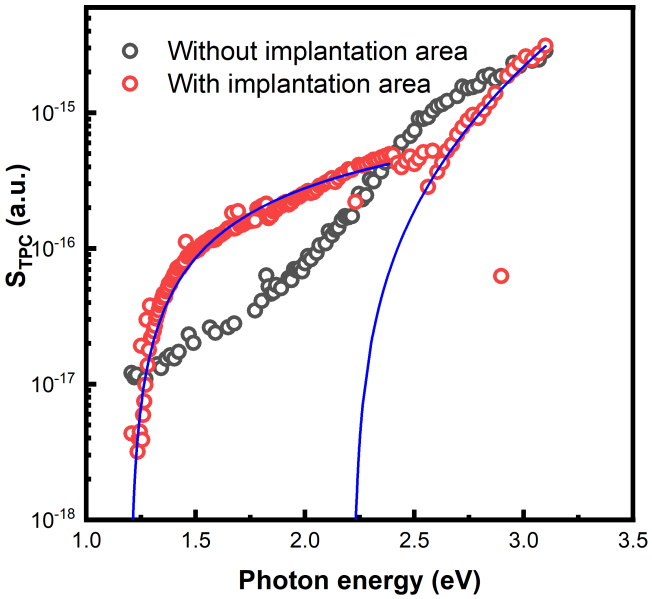
Without implantation area
With implantation area
10^{-15}
10^{-16}
10^{-17}
10^{-18}
S_{TPC} (a.u.)
1.0
1.5
2.0
2.5
3.0
3.5
Photon energy (eV)

Figure 4

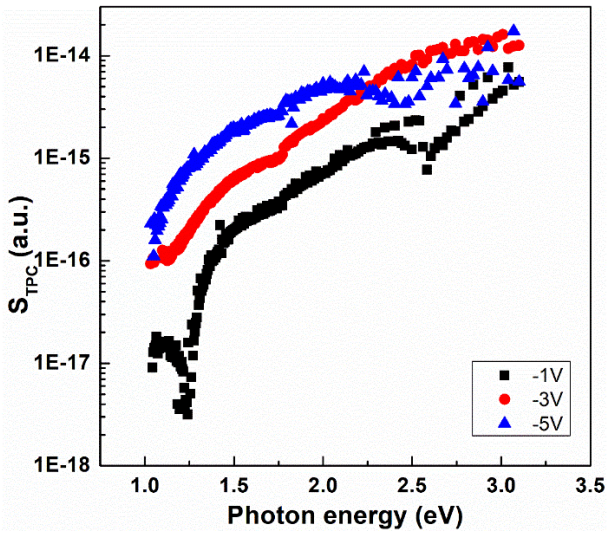
1E-14
1E-15
1E-16
1E-17
1E-18
S_{TPC} (a.u.)
1.0
1.5
2.0
2.5
3.0
3.5
Photon energy (eV)
-1V
-3V
-5V

Figure 5

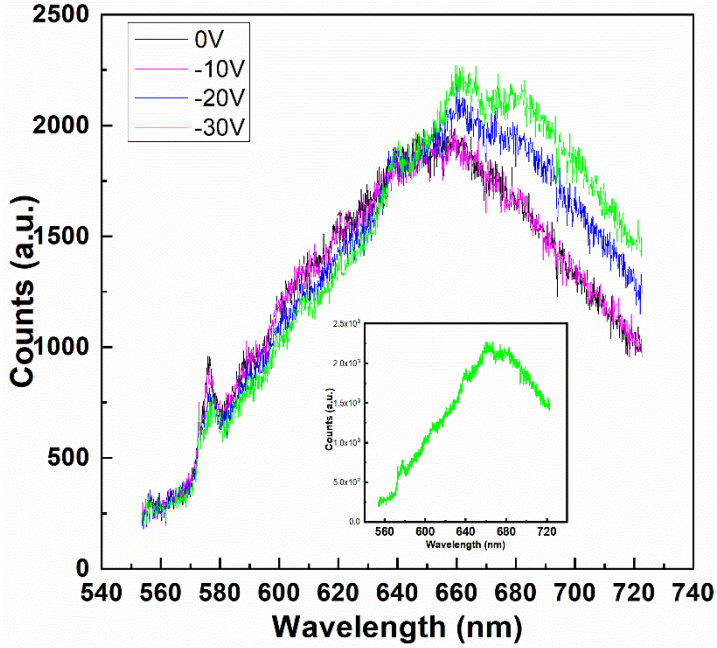
0V
-10V
-20V
-30V
Counts (a.u.)
Wavelength (nm)
2500
2000
1500
1000
500
0
540 560 580 600 620 640 660 680 700 720 740
Counts (a.u.)
Wavelength (nm)
560 600 640 680 720

Figure 6

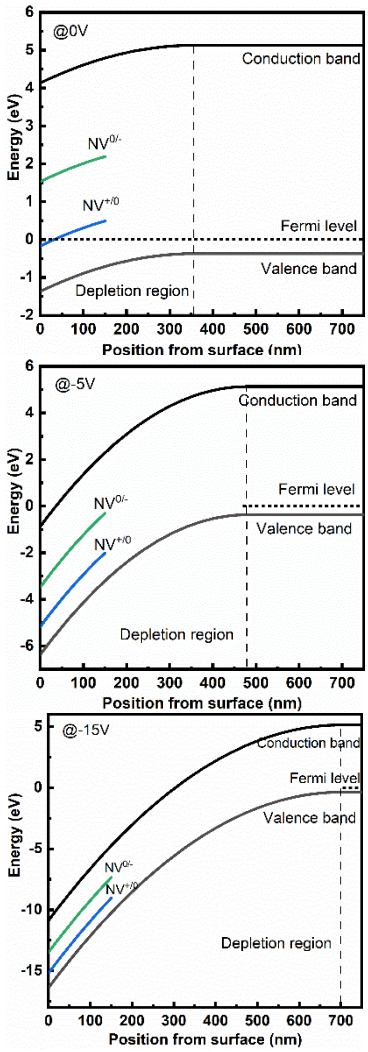
@0V
Conduction band
Fermi level
Valence band
Depletion region
Energy (eV)
Position from surface (nm)
@-5V
Conduction band
Fermi level
Valence band
Depletion region
Energy (eV)
Position from surface (nm)
@-15V
Conduction band
Fermi level
Valence band
Depletion region
Energy (eV)
Position from surface (nm)

Figure 7

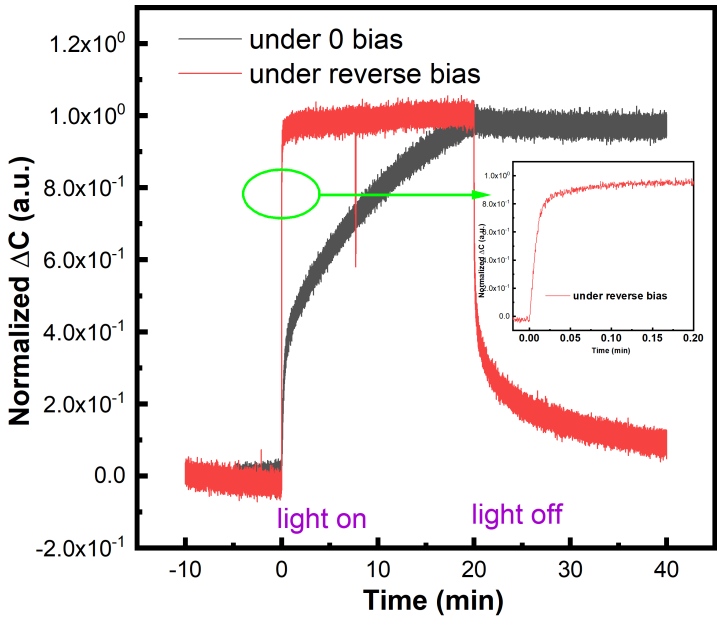
under 0 bias
under reverse bias
1.2x10^0
1.0x10^0
8.0x10^-1
6.0x10^-1
4.0x10^-1
2.0x10^-1
0.0
-2.0x10^-1
Normalized ΔC (a.u.)
light on
light off
-10
0
10
20
30
40
Time (min)
under reverse bias
Time (min)

Figure 8